The Iron–Sulfur Cluster in the Oxidized High-Potential Iron Protein from *Ectothiorhodospira halophila*

Lucia Banci,[†] Ivano Bertini,*[,†] Francesco Capozzi,[‡] Paolo Carloni,[†] Stefano Ciurli,[‡] Claudio Luchinat,[‡] and Mario Piccioli[†]

Contribution from the Department of Chemistry, University of Florence, Via Gino Capponi 7, 50121 Florence, Italy, and Institute of Agricultural Chemistry, University of Bologna, Viale Berti Pichat 10, 40127 Bologna, Italy

Received May 26, 1992

Abstract: In our efforts to characterize oxidized high-potential iron–sulfur proteins (HiPIP), we have investigated the oxidized HiPIP II from *Ectothiorhodospira halophila* through ^{1}H NMR and molecular dynamics (MD) calculations. This protein has the most symmetric isotropic shift pattern of the β-CH_2 protons of the liganded cysteines, four signals being upfield and four downfield. ^{1}H NOE, NOESY, and TOCSY results have provided the necessary key connectivities to perform the assignment of the liganded cysteines, taking advantage of the structure of the HiPIP I isoprotein. It is found that the electronic distribution within the cluster is different with respect to the *Chromatium vinosum* and *Rhodocyclus gelatinosus* systems. As in the latter systems, the cluster can be described in terms of two iron(III) and two mixed valence ions, but the two pairs are oriented in a different way within the protein frame. These results are discussed in terms of structure–function relationships. An MD approach starting from the structure of HiPIP I has provided a structural model of the present protein, which is absolutely consistent with the NMR connectivities in the surroundings of the cluster.

Introduction

High-potential iron–sulfur proteins (HiPIP hereafter) are a class of proteins containing a cluster $[Fe_4S_4]$ which, in the oxidized form, can be viewed as constituted by four iron(III) ions plus one extra electron.[1] Among the many possible electronic states for such a system, magnetic Mössbauer,[2] ^{1}H NMR investigations,[3] and theoretical studies[4] provide a picture consistent with two iron(III) ions and a mixed valence iron(III)–iron(II) pair. In this picture, the ground-state spin quantum number, $S = {}^1/_2$, can be viewed as constituted by two subspins, S_{12} and S_{34} for the ferric and mixed valence pair, respectively, which are antiferromagnetically coupled. It is found that $S_{34} > S_{12}$,[4e,5] the most likely values being ${}^9/_2$, 4 or ${}^7/_2$, 3.[4c–e,6]

The sequence-specific assignment of the ^{1}H NMR signals of the cysteines bound to each type of iron ion in HiPIP from *Chromatium vinosum*, which was possible because of the availability of its X-ray structure,[7] has allowed the framing of the cluster inside the protein.[8] A similar study is available for oxidized HiPIP from *Rhodocyclus gelatinosus* (formerly *Rhodopseudomonas gelatinosa*),[3b,9] which has a large homology with the HiPIP from *C. vinosum* in the vicinity of the cluster core[10] and whose NMR spectra are very similar to those of *C. vinosum* HiPIP. For both proteins it appears that the mixed valence pair is on the same two iron ions of the three that are closer to the surface of the protein whereas the third and the most buried iron ion are ferric.[8]

Recently, the X-ray structure of HiPIP I from *Ectothiorhodospira halophila* has been solved at 2.5-Å resolution.[10] Despite the fact that the sequence homology of this protein with the HiPIP from *C. vinosum* is rather low, the overall tertiary structures are surprisingly similar. In particular, there is strict structural correspondence between the cysteines coordinating the cluster in the two proteins (Figure 1). This piece of information allows us to state with some confidence that the same structural correspondence between the individual cysteines should exist for all other HiPIPs of known sequence. These correspondences are listed in Table I.

If so much is now known about the general structural features of this class of proteins, it is still not clear why there is such a resulting distribution of oxidation states in the cluster (i.e. a mixed valence pair and a ferric pair) with respect to the protein frame and whether this is a general feature of HiPIPs. Therefore, we have undertaken a further study of the HiPIP II from *E. halophila*, for which recent Mössbauer data indicate that, like in *C. vinosum* HiPIP, $S_{34} > S_{12}$.[11] This is a piece of information needed for the following NMR interpretation. This protein has the lowest reduction potential among HiPIPs and is the only one which shows four β-CH_2 protons downfield and four upfield.[12,13]

[†] University of Florence.
[‡] University of Bologna.

(1) (a) Carter, C. W. In *Iron-Sulfur Proteins III*; Lovenberg, W., Ed.; Academic Press: New York, 1977; p 157. (b) Thomson, A. J. *In Metalloproteins*; Harrison, P., Ed.; Verlag Chemie: Weinheim, Germany, 1985; p 79.

(2) (a) Moss, T. H.; Bearden, A. J.; Bartsch, R. G.; Cusanovich, M. A. *Biochemistry* **1968**, *7*, 1591. (b) Dickson, D. P. E.; Johnson, C. E.; Cammack, R.; Evans, M. C. W.; Hall, D. O.; Rao, K. K. *Biochem. J.* **1974**, *139*, 105.

(3) (a) Bertini, I.; Briganti, F.; Luchinat, C.; Scozzafava, A.; Sola, M. *J. Am. Chem. Soc.* **1991**, *113*, 1237. (b) Banci, L.; Bertini, I.; Briganti, F.; Luchinat, C.; Scozzafava, A.; Vicens Oliver, M. *Inorg. Chem.* **1991**, *30*, 4517.

(4) (a) Papaefthymiou, V.; Girerd, J. J.; Moura, I.; Moura, J. J. G.; Münck, E. *J. Am. Chem. Soc.* **1987**, *109*, 4703. (b) Münck, E.; Papaefthymiou, V.; Surerus, K. K.; Girerd, J. J. In *Metal Clusters in Proteins*; Que, L., Ed.; ACS Symposium Series 1987; American Chemical Society: Washington, DC, 1988; p 302. (c) Noodleman, L. *Inorg. Chem.* **1988**, *27*, 3677. (d) Banci, L.; Bertini, I.; Luchinat, C. *Struct. Bonding (Berlin)* **1990** *72*, 113. (e) Banci, L.; Bertini, I.; Briganti, F.; Luchinat, C. *New J. Chem.* **1991**, *15*, 467.

(5) Middleton, P.; Dickson, D. P. E.; Johnson, C. E.; Rush, J. D. *Eur. J. Biochem.* **1980**, *104*, 289.

(6) Mauesca, J. M.; Lamotte, B.; Rius, G. J. *Inorg. Biochem.* **1991**, *43*, 251.

(7) (a) Carter, C. W.; Kraut, J.; Freer, S. T.; Xuong, N.-H.; Alden, R. A.; Bartsch, R. G. *J. Biol. Chem.* **1974**, *249*, 4212. (b) Carter, C. W.; Kraut, J.; Freer, S. T.; Alden, R. A. *J. Biol. Chem.* **1974**, *249*, 6339.

(8) (a) Bertini, I.; Capozzi, F.; Ciurli, S.; Luchinat, C.; Messori, L.; Piccioli, M. *J. Am. Chem. Soc.* **1992**, *114*, 3332. (b) Nettesheim, D. G.; Harder, S. R.; Feinberg, B. A.; Otvos, J. D. *Biochemistry* **1992**, *31*, 1234.

(9) Bertini, I.; Capozzi, F.; Luchinat C.; Piccioli, M.; Vicens Oliver, M. *Inorg. Chim. Acta* **1992**, *198–200*, 483.

(10) Breiter, D. R.; Meyer, T. E.; Rayment, I.; Holden, H. M. *J. Biol. Chem.* **1991**, *266*, 18660.

(11) Bertini, I.; Campos, A. P.; Luchinat, C.; Teixeira, M. *J. Inorg. Biochem.*, in press.

(12) Krishnamoorthi, R.; Markley, J. L.; Cusanowich, M. A.; Prysiecki, C. T.; Meyer, T. E. *Biochemistry* **1986**, *25*, 60–67.

(13) Banci, L.; Bertini, I.; Briganti, F.; Luchinat, C.; Scozzafava, A.; Vicens Oliver, M. *Inorg. Chim. Acta* **1991**, *180*, 171.

0002-7863/93/1515-3431$04.00/0

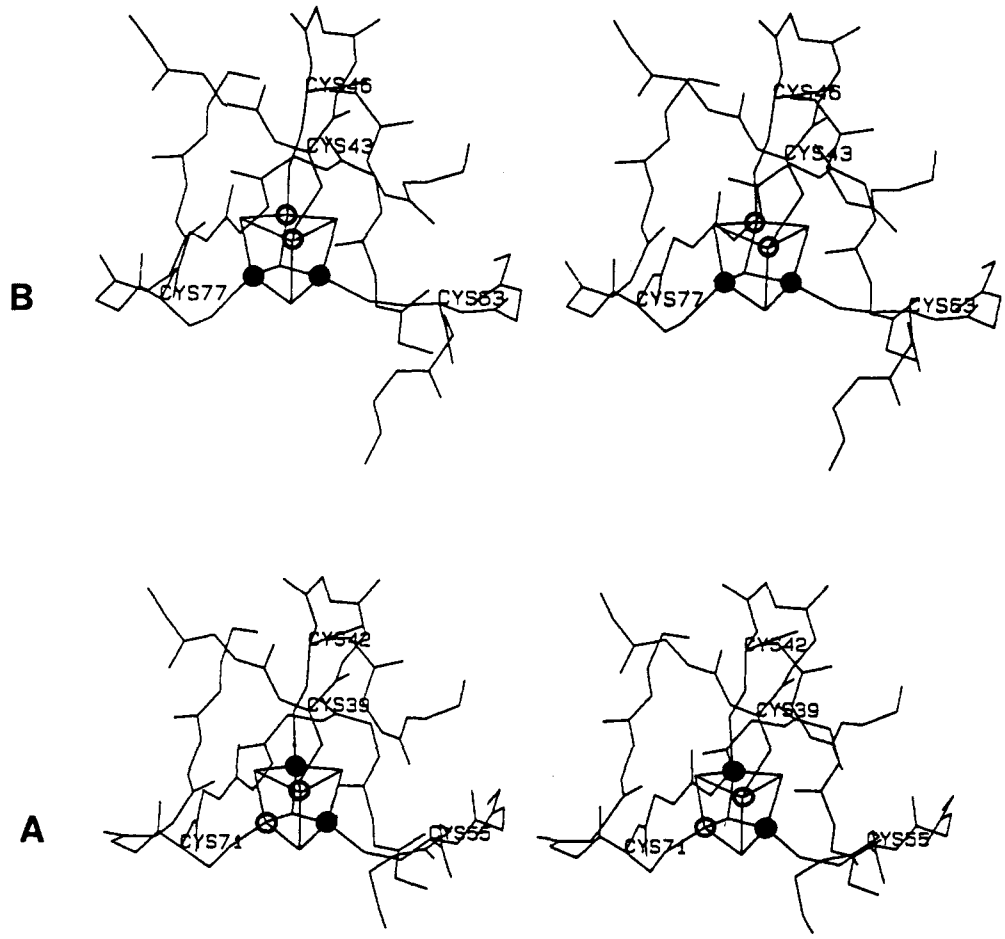

Figure 1. Stereoview of Fe–S cluster together with metal-coordinated cysteines of (A) *E. halophila* HiPIP II from MD simulation and (B) *C. vinosum* HiPIP from crystallographic data. White circles indicate Fe(3+) ions and black circles indicate Fe(2.5+) ions.

Table I. Correspondences of the Cysteine Residues among HiPIPs from Various Sources

residue number					
Cys I	Cys II	Cys III	Cys IV	HiPIP source	ref
43	46	63	77	*C. vinosum*	12
43	46	63	77	*T. roseopersicina*	12
43	46	61	75	*C. gracile*	12
43	46	59	73	*T. pfennigii*	12
36	39	53	67	*R. gelatinosum*	12
37	40	50	64	*Paracoccus* sp.	12
39	42	55	71	*E. halophila* II	12
31	34	48	64	*E. halophila* I	12
23	26	41	56	*Rs. tenue* 3761	12
21	24	39	54	*Rs. tenue* 2761	12
34	37	51	65	*E. vacuolata* I	39
34	37	51	65	*E. vacuolata* II	39
21	24	33	46	*R. globiformis*	39[a]

[a] Not yet finalized.

This is why it was chosen to be investigated by Mössbauer spectroscopy. All the other proteins investigated[3,8,9,12] have four downfield β-CH_2 proton signals but only two upfield β-CH_2 proton signals; however, two more downfield signals are present with anti-Curie temperature dependence. For this reason, the investigation of the sequence-specific assignment of this protein is particularly interesting.

The sequence-specific assignment was possible for the HiPIP from *C. vinosum* because from the X-ray structure it appeared that one β-CH_2 of Cys 43 was close to an α proton of an Ala and three peptide NH protons, one β-CH_2 of Cys 46 was close to a Trp NH, one β-CH_2 proton of Cys 63 was close to a β-methylene proton of a Phe, the β and the α protons of Cys 77 were close to the α protons of a Tyr, and the α proton of the same cysteine was close to two six-membered-ring protons of another Trp. The patterns of the Trp and Phe residues were recognized in the TOCSY spectra, and one or more signals of the pattern were dipolarly connected with the protons of the coordinated cysteines.

HiPIP II from *E. halophila* has a 65% homology with the HiPIP I from the same source.[14] By comparing the primary structures of HiPIP II with HiPIP I from *E. halophila* and with HiPIP from *C. vinosum*, it is easy to predict that Cys 39 (Cys 43 in *C. vinosum*) is close to Trp 55, Cys 42 (Cys 46 in *C. vinosum*) to Tyr 74, Cys 55 (Cys 63 in *C. vinosum*) to Val 65, and Cys 71 (Cys 77 in *C. vinosum*) to Trp 70. All of these residues are conserved in the two proteins from *E. halophila*.

If we are able, as we are going to show that we are, to recognize the above groups and to connect them with the cysteine ligand protons, we can perform the sequence-specific assignment of the same residues close to the cluster in a protein of unknown structure as long as the homology-based model is correct. Of course, if it is not correct, we would not find a consistent network of connectivities among signals. It should be stressed that some signals of the residues in the proximity of the cysteine ligands may be themselves broadened by the dipolar coupling with the unpaired electrons, thus making them distinguishable from the same residues located far away from the cluster. We have assigned, either totally or partially, *eighteen* residues around the cluster, of which *seventeen* are conserved. These include the four cluster-bound cysteines. From the NMR parameters of the latter, we have found that the valence distribution within the cluster in *E. halophila* HiPIP II is different from that of the two other proteins.

Quite independently, an MD study can be done on a protein

(14) Przysiecki, C. T.; Meyer, T. E.; Cusanovich, M. A. *Biochemistry* **1985**, *24*, 2542.

by starting from the X-ray structure of a largely homologous protein.[15] We have shown that, in the case of the protein from *C. vinosum*, the choice of the parameters for the MD is such that the X-ray structure is reproduced and even refined. We feel confident in using this approach because of the large tertiary-structure similarities among all HiPIPs. Most importantly, we can check the outcome of the calculations by comparison with the NMR data. Note that there may be many experimentally available inter-proton distances in a sphere of ≃15-Å diameter around the cluster, if the intrinsic geometric restrictions within a residue are also considered.

This dualistic approach may turn out to be a quick alternative to the unusual sequence-specific assignment which, for a protein of MW 10 000, would require an average of six months of work.[16]

Finally, we stress the point that this procedure (i.e. independent use of both NMR and MD) may provide information on proteins even larger than those that can be tackled by the standard procedures. For example, NMR studies are available for several peroxidases,[17-19] which have about 45 000 MW, for which relatively detailed assignments are obtained around the iron(III) ion on the basis of only one available X-ray structure.[20]

Experimental Section

Oxidized *E. halophila* HiPIP II was isolated and purified according to the general procedure outlined by Bartsch.[21] The operations of protein extraction and purification were carried out at 4 °C. Ultrafiltration was carried out using an Amicon YM5 membrane unless otherwise specified. Ion-exchange chromatography was performed using a DEAE-cellulose Whatman DE-52. Dialysis was done using a Spectra-Por 6 MWCO 1000. Cell paste (450 g), obtained from four 10-L batches of cultures of *E. halophila* DSM 244 (type strain), grown photoheterotrophically on succinate[22] and malate, was suspended in 1 L of phosphate buffer I (0.1 M, pH 7.1) and disrupted using a French press. The resulting suspension was centrifuged at 12 000 × g for 30 min, and the supernatant was further centrifuged at 190 000 × g for 2 h. The solution obtained (700 mL) was dialyzed overnight against 20 L of water and concentrated to 300 mL by ultrafiltration. The pH was adjusted to 7.5, and the extract was loaded onto an ion-exchange column equilibrated with phosphate buffer II (10 mM, pH 7.5). After being washed with 1 L of the same buffer, the column was eluted with 0.5 L of buffer II containing 0.6 M NaCl. The collected fractions were dialyzed for 6 h against buffer II. The solution contained in the dialysis membrane was loaded onto an ion-exchange column equilibrated with buffer II. The column was washed with 250 mL of buffer II containing 60 mM NaCl and then eluted with buffer II containing a linear gradient 60–600 mM NaCl. The brown-red band of HiPIP was eluted with 280 mM NaCl. The fractions containing the HiPIP were collected, diluted 1:10 with water, and concentrated to 200 mL by ultrafiltration. The pH was adjusted to 7.5, and the resulting solution was loaded onto an ion-exchange column equilibrated with buffer II containing 100 mM NaCl. After being washed with buffer II containing 150 mM NaCl, the column was eluted using a linear gradient 150–350 mM NaCl. The fractions in which HiPIP was present were concentrated by ultrafiltration to 70 mL, and the resulting solution was loaded on a 120 cm^3 DEAE-Sephadex column (Pharmacia A50) equilibrated with buffer II containing 300 mM NaCl. Elution with the same buffer afforded a sample of HiPIP which was concentrated by ultrafiltration. The final purity index, A_{280}/A_{480}, was 2.2.

At variance with other HiPIPs, and possibly due to its relatively low reduction potential of +50 mV, *E. halophila* HiPIP II is stable in the oxidized form. The reduced form can be obtained by treating the sample with solid sodium dithionite and is also stable in the absence of oxygen. Samples containing both oxidized and reduced forms can also be obtained by using substoichiometric amounts of sodium dithionite.

NMR spectra on partially reduced samples, obtained under the same conditions as described below, are a superposition of the spectra of the oxidized and reduced forms, indicating slow interconversion between the two species. This is a common feature of all the HiPIPs investigated up to now. In the present research, all the NMR experiments were performed on samples in which the reduced protein was below the limits of detection in the NMR spectra. In any case, given the slow exchange conditions, the presence of reduced protein does not have an influence on the NMR results for the oxidized form.

All NMR spectra have been recorded on samples obtained after five cycles of solvent exchange with deuterated buffer (phosphate 30 mM pH* 5.1, uncorrected for the isotope effect) using an ultrafiltration Amicon cell equipped with a YM2 membrane.

The NMR spectra were recorded on an AMX 600 Bruker spectrometer operating at 600.14 MHz proton Larmor frequency. The spectra were calibrated assigning a shift of 4.80 ppm, with respect to DSS, to the residual HDO signal at 300 K.

1D NOE difference spectra have been collected using the methodology previously described.[23] The NOE η_{ij}, experienced by observing proton i upon saturation of the signal of proton j is, at a first approximation[24]

$$\eta_{ij} = \frac{\sigma_{ij}}{\rho_i}$$

where ρ_i is the selective T_1^{-1} of the observed proton i and σ_{ij} is the cross relaxation rate, which is given by

$$\sigma_{ij} = -\left[\frac{\mu_0}{4\pi}\right]^2 \frac{\hbar^2 \gamma_N^4}{10 r_{ij}^6} \tau_c$$

where τ_c is given by the protein rotational correlation time and r_{ij} is the distance between protons i and j, while μ_0, $\hbar$ and γ_N have their usual meanings.

2D NOESY spectra were recorded in the phase-sensitive mode, with the sequence RD–90–t_1–90–t_m–90–AQ.[25] Five hundred and twelve experiments were performed in f_1 dimension, with an increment in t_1 of 55 μs, 336 scans per t_1 value, and 1024 data points in f_2. The repetition and mixing times were 220 and 30 ms, respectively.

2D TOCSY spectra were acquired with the RD–90–t_1–SL–MLEV17–SL–AQ pulse sequence, where SL denotes a spin lock field applied for a short time (typically 2.5 ms) along the x axis and MLEV17 is a composite pulse sequence.[26] One thousand twenty four experiments were performed with t_1 increments of 55 μs, 176 scans per t_1 value, and 2048 data points in f_2, with a repetition time of 300 ms. The mixing times ranged from 10 to 60 ms.

For both NOESY and TOCSY spectra, the data matrix was multiplied by a phase-shifted squared sine bell window function in both dimensions, prior to Fourier transformation. The standard BRUKER software package was used for data processing.

The minimization and MD calculations were performed with the AMBER 4.0 program package[27] on a IBM RISC 6000/520 computer. The starting structure of HiPIP II from *E. halophila* was constructed from the available X-ray structure of HiPIP I from *E. halophila*,[10] by substituting the different residues and inserting the further residues with the molecular graphics program SYBYL.[28] The computational meth-

(15) (a) Paulsen, M. D.; Ornstein, R. L. *Proteins: Struct., Funct., Genet.* **1991**, *11*, 184–204. (b) Tirado-Rives, J.; Jorgensen, W. L. *J. Am. Chem. Soc.* **1990**, *112*, 2773–2781. (c) Stewart, D. E.; Wempler, J. E. *Proteins: Struct., Funct., Genet.* **1991**, *11*, 142–152.

(16) Wagner, G. *Prog. Nucl. Magn. Reson. Spectrosc.* **1990**, *22*, 101–139.

(17) (a) de Ropp, J. S.; La Mar, G. N. *J. Am. Chem. Soc.* **1991**, *113*, 4348. (b) de Ropp, J. S.; La Mar, G. N.; Wariishi, H.; Gold, M. H. *J. Biol. Chem.* **1991**, *266*, 15001.

(18) (a) Satterlee, J. D.; Erman, J. E. *Biochemistry*, **1991**, *30*, 4398. (b) Satterlee, J. :.; Russell, D. J.; Erman, J. E. *Biochemistry*, **1991**, *30*, 9072.

(19) (a) Banci, L.; Bertini, I.; Turano, P.; Tien, M.; Kirk, T. K. *Proc. Natl. Acad. Sci. U.S.A.* **1991**, *88*, 6956–6960. (b) Banci, L.; Bertini, I.; Turano, P.; Ferrer, G. C.; Mauk, A. G. *Inorg. Chem.* **1991**, *30*, 4510–45516. (c) Banci, L.; Bertini, I.; Pease, E.; Turano, P.; Tien, M. *Biochemistry* **1992**, *31*, 10009.

(20) Poulos, T. L.; Kraut, J. *J. Biol. Chem.* **1980**, *255*, 8199.

(21) Bartsch, R. G. *Methods Enzymol.* **1978**, *53*, 329.

(22) DSM—Deutsche Sammlung von Mikroorganismen und Zellkulturen GmbH.

(23) (a) Johnson, R. D.; Ramaprasad, S.; La Mar, G. N. *J. Am. Chem. Soc.* **1983**, *105*, 7205. (b) Banci, L.; Bertini, I.; Luchinat, C.; Piccioli, M.; Scozzafava, A.; Turano, P. *Inorg. Chem.* **1989**, *28*, 4650. (c) Lecomte, J. T. J.; Unger, S. W.; La Mar, G. N. *J. Magn. Reson.* **1991**, *94*, 112.

(24) (a) Noggle, J. H.; Shirmer, R. E. *The Nuclear Overhauser Effect*; Academic Press: New York, 1971. (b) Neuhaus, D.; Williamson, M. *The Nuclear Overhauser Effect in Structural and Conformational Analysis*; VCH: New York, 1989.

(25) Macura, S. R.; Ernst, R. R. *Mol. Phys.* **1980**, *40*, 95.

(26) Davis, D. G.; Bax, A. *J. Am. Chem. Soc.* **1985**, *107*, 2820.

(27) Pearlman, D. A.; Case, D. A.; Caldwell, J. C.; Seibel, G. L.; Chandra Singh, U.; Weiner, P.; Kollman, P. A. *AMBER 4.0*; University of California: San Francisco, CA, 1991.

(28) SYBYL Molecular *Modeling Software*. Tripos Associates, Inc., Evans & Sutherland, 1699 S. Hanley Rd., St. Louis, MO.

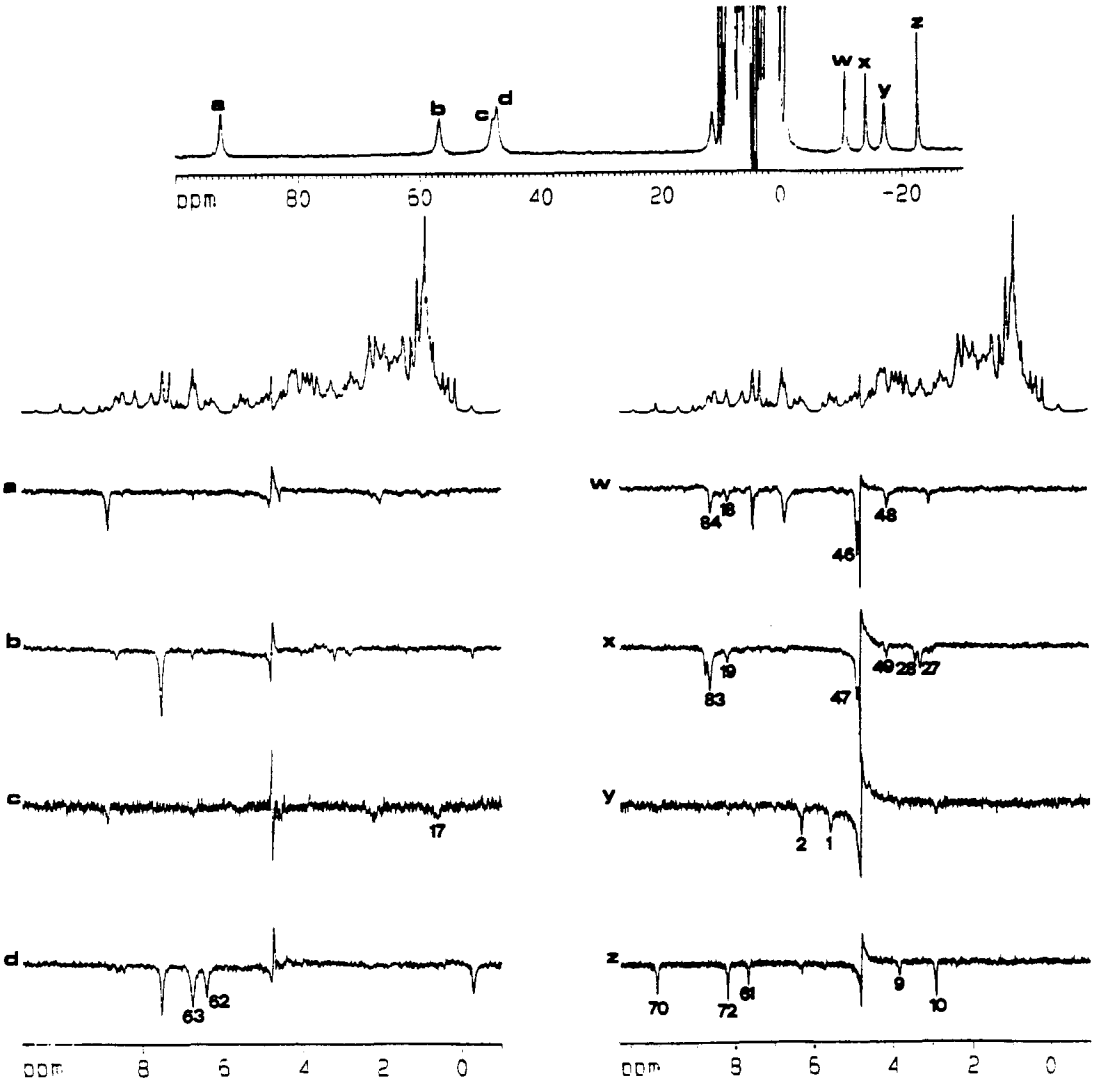

Figure 2. ^{1}H NOE difference spectra (600 MHz, 300 K) of oxidized *E. halophila* HiPIP II obtained upon saturation of the hyperfine shifted signals. The region 11 to −1 ppm of the NOE difference spectra is shown. The ^{1}H NMR spectrum is shown in the upper part of the figure. Traces are labeled according to the saturated signal. The saturation time was 80 ms. The difference spectra are scaled in a way such that the areas of the saturated signals are all equal.

odology corresponds to those described previously[29] except as noted below. The force field parameters for all the residues except the iron–sulfur cluster and the cysteine ligands to the iron ions are the standard AMBER "all atoms" parameters.[30] For the Fe–S cluster we used the force field parameters already developed for describing HiPIP from *C. vinosum*.[29] The overall charge of the protein (−11 at physiological pH) was neutralized[31] by adding 11 sodium ions. The final model consisted of 5332 atoms including the addition of 1393 water molecules.

The entire system was minimized, after the minimization and equilibration of the water molecules, with 9 ps of dynamics. Finally, MD calculations were performed by slowly warming up the whole system from 0 to 300 K in seven steps (0–10, 10–50, 50–100, 100–150, 150–200, 200–250, 250–300) each of the duration of 1.8 ps. The trajectory was performed for a total of 147 ps. The first 40 ps were discarded, and the structures calculated during the last 107 ps were used to generate an average structure for analysis of the NOE data.

Results

Assignment of Cysteines. The ^{1}H NMR spectrum of oxidized HiPIP II from *E. halophila* is reported in Figure 2. Mössbauer data show strict analogies between the cluster in the present system and that in *C. vinosum*, with the mixed valence pair having a spin substate larger than that of the other pair of iron(III) ions, and very similar hyperfine constants.[11] It follows that the ^{1}H NMR signals of the β-CH_2 protons of the cysteines bound to the iron ions of the mixed valence pair are shifted downfield, whereas the ones corresponding to the iron ions of the ferric pair are shifted upfield. This behavior arises because of the contact contribution to the hyperfine shift,[3b,4d,e,8,9] which is always dominating for β-CH_2 protons in these systems.[32] The geminal nature of the protons had been recognized through NOE measurements.[13] The results of such experiments are shown in Figure 2, which reports the diamagnetic region of the ^{1}H NOE difference spectra obtained by saturating the eight hyperfine shifted signals.

In order to reach the assignment listed in Table II, we will refer in the following to the proton–proton connectivities reported in Table III. In this table the inter-proton distances as obtained from MD calculations (see later) are also reported. As already stated, these distances have not been used to arrive at the sequence-specific assignment. The connectivities are numbered sequentially in Table III, and the same numbers are used in Figures 2–4.

By saturating the β-CH_2 signal y, an NOE is observed on two signals at 6.30 (connectivity 2, according to Figure 2y and Table

(29) Banci, L.; Bertini, I.; Carloni, P.; Orioli, P. L. *J. Am. Chem. Soc.* **1992**, *114*, 10683.
(30) Weiner, S. J.; Kollman, P. A.; Case, D. A.; Chandra Singh, U.; Ghio, A.; Alagona, G.; Profeta, S.; Weiner, P. *J. Am. Chem. Soc.* **1984**, *106*, 765.
(31) Rao, G. B.; Slingh, U. C. *J. Am. Chem. Soc.* **1991**, *113*, 6735.
(32) Reynolds, J. G.; Laskowsky, E. J.; Holm, R. H. *J. Am. Chem. Soc.* **1978**, *100*, 5315.

Table II. Assignment of the Cysteine Protons in Oxidized HiPIP II from *E. halophila*

residue	proton	signal	δ (ppm)
cysteine 39	β_1	z	−22.66
	β_2	y	−17.22
	α		
cysteine 42	β_1	d	47.16
	β_2	b	56.72
	α		7.55
cysteine 55	β_1	c	47.85
	β_2	a	92.52
	α		
cysteine 71	β_1	x	−14.24
	β_2	w	−10.84
	α		8.65

III) and 5.58 (1) ppm. The TOCSY map (Figure 3), which reveals through-bond connectivities, shows that these signals belong to a Trp residue (3–7). The NOESY (Figure 4) and TOCSY maps allow us to assign them as $H\zeta_3$ and $H\epsilon_3$, respectively. By inspecting the structure of the isoprotein I, Trp 45 is located in such a way that the $H\zeta_3$ and $H\epsilon_3$ are located close to Cys 39 $H\beta_2$. Signal y is therefore $H\beta_2$ of Cys 39. Chemical shift values of Trp 45 protons are 1–2 ppm upfield with respect to usual shifts of Trp proton resonances. Ring current effects due to the various aromatic residues around Trp 45 can rationalize this finding. One of the connectivities (8, Table III) of the spin pattern of Trp 45 is missing presumably because the relative $H\epsilon_3$ is close to the paramagnetic center. Despite that, the assignment to a Trp residue is sound because no other residue is consistent with the pattern in Figure 3. $H\beta_1$ of Cys 39 (signal z) gives NOE (Figure 2z) with two signals at 3.84 (9) and 2.93 (10) ppm, which have shifts and a TOCSY pattern (11 in Table III, not shown in Figure 3) consistent with Hα of a Gly. They are assigned as $H\alpha_1$ and $H\alpha_2$ of Gly 67, respectively. This is the only nonconserved residue among those considered in the present assignment. Gly 67 replaces Ala 67 in HiPIP II. The NH of Gly 67 is assigned from the TOCSY experiment (not shown) to a signal at 8.93 ppm, which also gives NOESY cross peaks with both α protons (12, 13, Figure 4). Finally, $H\alpha_2$ of Gly 67 shows a NOESY connectivity with $H\zeta_3$ and Hη of Trp 45 (14, 15, Figure 4), confirming the whole pattern of connectivities in this region. As already discussed in the introduction, signals y and z belong to a cysteine bound to iron(III). Therefore, Cys 39 is bound to an iron(III) ion.

When either signal w or x (two β-CH_2 belonging to the same crysteine) is saturated, a NOE is observed on a signal in the aromatic region at 8.20 ppm (18, 19, Figure 2w,x), which is part of the NOESY and TOCSY patterns of a Phe residue (20–22, Figure 3, and 21, 22, Figure 4). The only Phe residue close to the cluster is Phe 60, and therefore w and z are assigned as Cys 71 β-CH_2. Both signals w and z give NOE with a signal at 8.65 ppm (83, 84), which experiences a strong anti-Curie temperature dependence typical of a cysteine residue bound to an iron of the ferric pair, and therefore the latter signal is assigned to Hα of Cys 71. The two β-CH_2 protons of Cys 71 give NOE (46, 47), and the α CH gives NOESY (45) with a signal at 4.90 ppm. This signal is dipolarly and scalarly coupled with the two protons of a β CH_2 (43, 44) and a peptide NH (50), and is therefore assigned to an α proton which likely belongs to Tyr 20 (see also further assignments). The $H\beta_1$ of this residue shows NOE with w and z (48, 49, Figure 2w,x). From the connectivity patterns observed upon saturation of Cys 71 geminal protons, we can assign signals x and w as $H\beta_1$ and $H\beta_2$, respectively. Again, from the chemical shift of signals w and x, Cys 71 is bound to an iron(III) ion.

Among the methylene protons of the two cysteines not yet assigned, only $H\beta_1$ of Cys 42 is expected to give strong NOEs with aromatic signals and in particular with Hδ and Hε of Tyr 74. By saturating signals a–d, only in the case of signal d is NOE observed with two signals in the aromatic region at 6.80 and 6.42 ppm (62, 63, Figure 2d), which are dipolarly and scalarly coupled (64, Figure 3 and 4). Thus, signals d and b are assigned as Cys 42 $H\beta_1$ and $H\beta_2$, respectively.

Little is learned by saturating signals a and c of the remaining cysteine, which, by exclusion, is Cys 55. Thus, Cys 42 and Cys 55 are coordinated to the mixed valence pair.

Further Assignments. Further assignments can be made, which provide support for the above site-specific assignment or are at least consistent with it. These assignments are also collected in Table III. All the residues involved are conserved on passing from HiPIP I to HiPIP II.

Signal x ($H\beta_1$ Cys 71) gives two NOEs at 3.30 (27) and 3.43 (28) ppm (Figure 2x), which could reasonably be assigned to β-CH_2 of His 18, as indicated by the NOESY map (26, not shown). A NOESY connectivity is observed (24) from the signal at 3.30 ppm and a signal at 6.69 ppm, assigned as His 18 $H\delta_2$. The latter shows a NOESY cross peak (23) with a signal already assigned as Hε of Phe 60 (7.79 ppm), which in turn is weakly dipolarly coupled (38) with His 18 $H\beta_1$ (3.30 ppm). $H\zeta$ and Hε of Phe 60 are close to $H\beta_1$ of Tyr 20, already assigned at 4.13 ppm (40, 41). Furthermore, the Hε of Phe 60 is dipolarly connected (29) with a methyl group at −1.13 ppm, whose NOESY and TOCSY patterns are typical of a Val residue (not shown). We assign it as Val 73.

From Figure 2z it appears that, by saturating Cys 39 $H\beta_1$, three more NOEs are observed. Two of them (at 10.05 (70) and 8.20 (72) ppm) have different intensities in H_2O and D_2O and are assigned as NH's. Because they are also dipolarly connected each other (71), they can be assigned as Cys 39 and Glu 40 peptide NH's. The third signal, at 7.67 ppm (61), is assigned as the NH proton of a Gly residue from its TOCSY pattern. This signal shows J coupling with the corresponding α protons (3.60 (59) and 3.87 (60) ppm, not shown in Figure 3) which are both dipolarly connected to the peptide NH of Trp 70 at 8.14 ppm (57, 58). On the basis of the distances reported in Table III, we assign this signal as the Gly 69 NH proton. In turn, the signal of the peptidic NH of Trp 70 shows a NOESY cross peak at 0.74 ppm (56), belonging to a Val residue (Val 21) which is recognized by its TOCSY pattern. Finally, a NOESY connectivity is observed (51), consistent with Table III, between the peptide NH of Val 21 (8.37 ppm) and the Hα of Tyr 20 (4.90 ppm), which had already been assigned through NOE with the β-CH_2 and Hα of Cys 71, thus providing internal consistency.

The signal at 10.05 ppm (Cys 39 NH) is dipolarly connected (69) with a signal at 5.73 ppm, which gives TOCSY (68) with another signal at 8.48 ppm. Their chemical shifts and the observed connectivities suggest their assignment as the Hα and NH protons, respectively. The most reasonable candidate from the inspection of the structure of HiPIP I from *E. halophila* is Leu 38. The Leu 38 NH is then dipolarly connected with two aromatic protons (65, 66) already assigned (through saturation of signal d) as Tyr 74 protons. The Hα of Leu 38 gives a NOESY cross peak with a signal at 7.17 ppm (73), which is part of a Trp residue assigned as Trp 70. The $H\epsilon_3$ of Trp 70 (7.07 ppm) is dipolarly coupled (82) with the Cys 71 Hα (8.65 ppm).

Finally, two further signals can be tentatively assigned on the basis of the observed NOEs. The assignment of the individual Hβ protons of Cys 55 is performed on the basis of their relative T_1 and T_2 values.[13] The NOE at 8.48 ppm observed when irradiating signals a and c (Figure 2a,c) is tentatively assigned to the Cys 55 NH. Furthermore, an NOE is observed on a signal at 0.61 ppm when saturating c (17), and the former signal gives a NOESY cross peak (16) with the Trp 45 $H\zeta_3$ (6.30 ppm). This is consistent with the assignment of the signal at 0.61 ppm as CH_3 of Val 65. There is no evidence that allows the definite assignment of the Cys 55 Hα.

The Hα of Cys 42 is probably the signal at 7.55 ppm, observed

Table III. Proton–Proton Connectivities and Signal Assignments Obtained from NMR Data on HiPIP II from *E. halophila* and MD-Derived Distances (Labels Refer to the Connectivities Reported in Figures 2–4)

Connectivity*	Label	Type	Distance (Å)
−17.22 (y) ⟶ Cys−39 Hβ2 — 5.58 Trp−45 Hε3	1	NOE	2.6 (± 0.3)
−17.22 (y) ⟶ Cys−39 Hβ2 — 6.30 Trp 45 Hζ3	2	NOE	3.6 (± 0.4)
6.30 Trp−45 Hζ3 ⟷ 5.58 Trp−45 Hε3	3	NOESY, TOCSY	2.4 (± 0.1)
6.30 Trp−45 Hζ3 ⟷ 6.38 Trp−45 Hη	4	NOESY[a], TOCSY	2.4 (± 0.1)
6.38 Trp−45 Hη ⟷ 4.88 Trp−45 Hζ2	5	NOESY, TOCSY	2.4 (± 0.1)
6.38 Trp−45 Hη ⟷ 5.58 Trp−45 Hε3	6	TOCSY	4.3 (± 0.1)
6.30 Trp−45 Hζ3 ⟷ 4.88 Trp−45 Hζ2	7	TOCSY	4.3 (± 0.1)
4.88 Trp−45 Hζ2 ⟷ 5.58 Trp−45 Hε3	8	[b]	5.0 (± 0.1)
−22.66 (z) ⟶ Cys−39 Hβ1 — 3.84 Gly−67 Hα1	9	NOE	4.1 (± 0.1)
−22.66 (z) ⟶ Cys−39 Hβ1 — 2.93 Gly−67 Hα2	10	NOE	3.2 (± 0.3)
3.84 Gly−67 Hα1 ⟷ 2.93 Gly−67 Hα2	11	NOESY[c], TOCSY[c]	1.7 (± 0.1)
3.84 Gly−67 Hα1 ⟷ 8.93 Gly−67 NH	12	NOESY, TOCSY[c]	2.7 (± 0.1)
2.93 Gly−67 Hα2 ⟷ 8.93 Gly−67 NH	13	NOESY, TOCSY[c]	2.2 (± 0.1)
2.93 Gly−67 Hα2 ⟷ 6.30 Trp−45 Hζ3	14	NOESY	2.9 (± 0.3)
2.93 Gly−67 Hα2 ⟷ 6.38 Trp−45 Hη	15	NOESY	3.2 (± 0.4)
6.30 Trp−45 Hζ3 ⟷ 0.61 Val−65 Hγ2	16	NOESY	2.4 (± 0.3)
0.61 Val−65 Hγ2 ⟵ 47.85 (c) Cys−55 Hβ1	17	NOE	2.8 (± 0.1)
−10.84 (w) ⟶ Cys−71 Hβ2 — 8.20 Phe−60 Hζ	18	NOE	2.6 (± 0.2)
−14.24 (x) ⟶ Cys−71 Hβ1 — 8.20 Phe−60 Hζ	19	NOE	2.6 (± 0.3)
8.20 Phe−60 Hζ ⟷ 6.21 Phe−60 Hδ	20	TOCSY	4.3 (± 0.1)
6.21 Phe−60 Hδ ⟷ 7.79 Phe−60 Hε	21	NOESY,TOCSY	2.4 (± 0.1)
7.79 Phe−60 Hε ⟷ 8.20 Phe−60 Hζ	22	NOESY,TOCSY	2.4 (± 0.1)
7.79 Phe−60 Hε ⟷ 6.69 His−18 Hδ2	23	NOESY	2.7 (± 0.3)
6.69 His−18 Hδ2 ⟷ 3.30 His−18 Hβ1	24	NOESY	2.6 (± 0.1)
6.69 His−18 Hδ2 ⟷ 3.43 His−18 Hβ2	25	[b]	3.7 (± 0.1)
3.30 His−18 Hβ1 ⟷ 3.43 His−18 Hβ2	26	NOESY[c]	1.7 (± 0.1)
3.30 His−18 Hβ1 ⟵ −14.24 (x) Cys−71 Hβ1	27	NOE	2.7 (± 0.3)
3.43 His−18 Hβ2 ⟵ −14.24 (x) Cys−71 Hβ1	28	NOE	3.6 (± 0.3)
7.79 Phe−60 Hε ⟷ −1.13 Val−73 Hγ2	29	NOESY	3.1 (± 0.3)
−1.13 Val−73 Hγ2 ⟷ 0.14 Val−73 Hγ1	30	NOESY[c]	2.5 (± 0.2)
−1.13 Val−73 Hγ2 ⟷ 1.70 Val−73 Hβ	31	NOESY[c]	2.3 (± 0.1)
−1.13 Val−73 Hγ2 ⟷ 8.48 Val−73 NH	32	NOESY	2.4 (± 0.2)
0.14 Val−73 Hγ1 ⟷ 1.70 Val−73 Hβ	33	NOESY[c], TOCSY[c]	2.3 (± 0.1)
1.70 Val−73 Hβ ⟷ 4.36 Val−73 Hα	34	NOESY[c], TOCSY[c]	2.4 (± 0.1)
4.36 Val−73 Hα ⟷ 0.14 Val−73 Hγ1	35	NOESY[c]	2.4 (± 0.2)
4.36 Val−73 Hα ⟷ 8.48 Val−73 NH	36	NOESY[c], TOCSY	2.9 (± 0.1)
−1.13 Val−73 Hγ ⟷ 6.69 His−18 Hδ2	37	NOESY.	3.3 (± 0.4)
7.79 Phe−60 Hε ⟷ 3.30 His−18 Hβ1	38	NOESY	3.2 (± 0.3)
3.30 His−18 Hβ1 ⟷ 8.20 Phe−60 Hζ	39	NOESY	3.4 (± 0.5)
8.20 Phe−60 Hζ ⟷ 4.13 Tyr−20 Hβ1	40	NOESY	2.2 (± 0.2)
4.13 Tyr−20 Hβ1 ⟷ 7.79 Phe−60 Hε	41	NOESY	2.8 (± 0.4)
4.13 Tyr−20 Hβ1 ⟷ 3.08 Tyr−20 Hβ2	42	NOESY[c], TOCSY[c]	1.7 (± 0.1)
3.08 Tyr−20 Hβ2 ⟷ 4.90 Tyr−20 Hα	43	NOESY, TOCSY[c]	2.9 (± 0.1)
4.90 Tyr−20 Hα ⟷ 4.13 Tyr−20 Hβ1	44	NOESY, TOCSY[c]	2.4 (± 0.1)
4.90 Tyr−20 Hα ⟷ 8.65 Cys−71 Hα	45	NOESY	2.5 (± 0.2)
4.90 Tyr−20 Hα ⟵ −10.84 (w) Cys−71 Hβ2	46	NOE	2.9 (± 0.2)
4.90 Tyr−20 Hα ⟵ −14.24 (x) Cys−71 Hβ1	47	NOE	3.2 (± 0.3)
4.13 Tyr−20 Hβ1 ⟵ −10.84 (w) Cys−71 Hβ2	48	NOE	3.1 (± 0.4)
4.13 Tyr−20 Hβ1 ⟵ −14.24 (x) Cys−71 Hβ1	49	NOE	2.9 (± 0.4)
4.90 Tyr−20 Hα ⟷ 7.53 Tyr−20 NH	50	NOESY, TOCSY	2.7 (± 0.4)
4.90 Tyr−20 Hα ⟷ 8.37 Val−21 NH	51	NOESY	2.2 (± 0.1)
8.37 Val−21 NH ⟷ 4.55 Val−21 Hα	52	NOESY, TOCSY	2.9 (± 0.1)
4.55 Val−21 Hα ⟷ 1.90 Val−21 Hβ	53	TOCSY[c]	2.5 (± 0.1)
1.90 Val−21 Hβ ⟷ 0.74 Val−21 Hγ2	54	TOCSY[c]	2.4 (± 0.1)
1.90 Val−21 Hβ ⟷ 0.90 Val−21 Hγ1	55	TOCSY[c]	2.4 (±0.1)
0.74 Val−21 Hγ2 ⟷ 8.14 Trp−70 NH_p	56	NOESY	3.0 (± 0.4)
8.14 Trp−70 NH_p ⟷ 3.60 Gly−69 Hα2	57	NOESY	2.5 (± 0.1)
8.14 Trp−70 NH_p ⟷ 3.87 Gly−69 Hα1	58	NOESY	2.7 (± 0.1)
3.60 Gly−69 Hα2 ⟷ 7.67 Gly−69 NH	59	TOCSY	2.3 (± 0.1)
7.67 Gly−69 NH ⟷ 3.87 Gly−69 Hα1	60	TOCSY	2.9 (± 0.1)
7.67 Gly−69 NH ⟵ −22.66 (z) Cys−39 Hβ1	61	NOE	2.9 (± 0.3)
47.16 (d) ⟶ Cys−42 Hβ1 — 6.42 Tyr−74 Hε	62	NOE	2.7 (± 0.3)
47.16 (d) ⟶ Cys−42 Hβ1 — 6.80 Tyr−74 Hδ	63	NOE	2.6 (±0.3)
6.80 Tyr−74 Hδ ⟷ 6.42 Tyr−74 Hε	64	NOESY, TOCSY	2.5 (± 0.1)
6.42 Tyr−74 Hε ⟷ 8.48 Leu−38 NH	65	NOESY	3.3 (± 0.4)
8.48 Leu−38 NH ⟷ 6.80 Tyr−74 Hδ	66	NOESY	4.8 (± 0.1)
8.48 Leu−38 NH ⟷ 4.14 Gln−37 Hα	67	NOESY	2.3 (± 0.1)
8.48 Leu−38 NH ⟷ 5.73 Leu−38 Hα	68	TOCSY	2.9 (± 0.1)
5.73 Leu−38 Hα ⟷ 10.05 Cys−39 NH	69	NOESY	2.3 (± 0.1)
10.05 Cys−39 NH ⟵ −22.66 (z) Cys−39 Hβ1	70	NOE	2.5 (± 0.2)
10.05 Cys−39 NH ⟷ 8.20 Glu−40 NH	71	NOESY	2.9 (± 0.2)
8.20 Glu−40 NH ⟵ −22.66 (z) Cys−39 Hβ1	72	NOE	2.7 (± 0.2)
5.73 Leu−38 Hα ⟷ 7.17 Trp−70 Hδ	73	NOESY	3.6 (± 0.4)
7.17 Trp−70 Hδ ⟷ 10.17 Trp−70 NH	74	NOESY	2.5 (± 0.1)
10.17 Trp−70 NH ⟷ 7.42 Trp−70 Hζ2	75	NOESY	2.9 (± 0.1)
7.42 Trp−70 Hζ2 ⟷ 6.78 Trp−70 Hη	76	NOESY, TOCSY	2.4 (± 0.1)
6.78 Trp−70 Hη ⟷ 6.82 Trp−70 Hζ3	77	NOESY[a], TOCSY[a]	2.4 (± 0.1)
6.82 <rp−70 Hζ3 ⟷ 7.07 Trp−70 Hε3	78	NOESY, TOCSY	2.4 (± 0.1)
6.82 Trp−70 Hζ3 ⟷ 7.42 Trp−70 Hζ2	79	TOCSY	4.3 (± 0.1)
6.78 Trp−70 Hη ⟷ 7.07 Trp−70 Hε3	80	TOCSY	4.3 (± 0.1)
7.07 Trp−70 Hε3 ⟷ 7.42 Trp−70 Hζ2	81	TOCSY	5.0 (± 0.1)
7.07 Trp−70 Hε3 ⟷ 8.65 Cys−71 Hα	82	NOESY	3.2 (± 0.3)
8.65 Cys−71 Hα ⟵ −14.24 (x) Cys−71 Hβ1	83	NOE	2.3 (± 0.1)
8.65 Cys−71 Hα ⟵ −10.84 (w) Cys−71 Hβ2	84	NOE	2.5 (± 0.1)

* The number above the proton label is its chemical shift (in ppm) measured at 300 K at pH* 5.1. [a] Not resolved. [b] Not observed. [c] Not shown in the figures.

when irradiating signals b and d (Figure 2b and d). The Cys 39 Hα could be broad beyond detection because of its proximity to the cluster.

A comment is due on the hyperfine shift and temperature dependence of the signal assigned as the Hα of Cys 71 (8.65 ppm). At variance with the corresponding β-CH_2 (signals w and x), the signal experiences a downfield shift. Nevertheless its temperature dependence is anti-Curie, which is in agreement

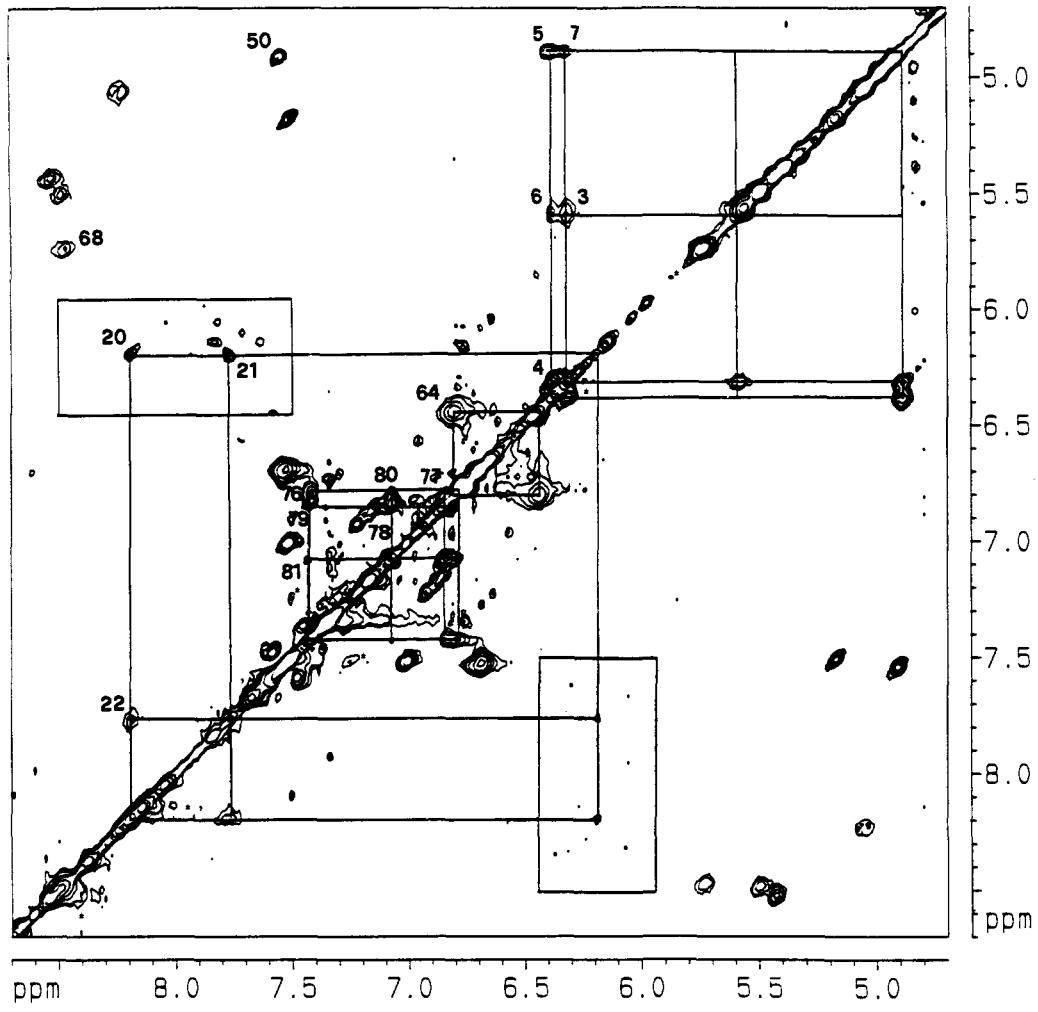

Figure 3. ^{1}H NMR TOCSY spectrum (600 MHz, 300 K) of the oxidized HiPIP II from *E. halophila*. Only the aromatic region is shown. The patterns of Trp 45, Trp 70, Phe 60, and Tyr 74 are indicated. Labeling of the observed cross peaks is reported according to Table III. Conditions as reported in the experimental section. The insets have been processed using 512 × 512 data points, zero filled to 1K × 1K data points. A $\pi/4$-shifted squared sine bell window function was applied in both dimensions.

with the pseudo-Curie behavior of its β-CH_2, on the basis of the theoretical model developed for these systems.[4c,d,8,9] While the temperature dependence unequivocally confirms its belonging to a cysteine coordinated to one of the ferric ions, the downfield shift is not readily understood. Among various possibilities, an explanation could be that for this particular proton a sizable dipolar shift contribution is present. A downfield dipolar shift on this proton could account for both a large downfield shift in those HiPIPs where the contact shift is downfield and a small residual downfield shift at room temperature in the present HiPIP, where the contact shift is upfield.

MD Results and Consistency of the Whole Picture. The starting *E. halophila* HiPIP II structure was generated by amino acid replacements and additions on the X-ray coordinates of *E. halophila* HiPIP I, as described in the Experimental Section. Minimization of this starting structure produced only minor changes, while substantial changes occurred during the first 20 ps of dynamics. After less than 40 ps, the protein assumed a stable structure, which was then maintained along the rest of the trajectory. The MD trajectory was calculated for a total of 147 ps. We have chosen to perform such a long calculation, as we start from a structure partially model-built, and we are calculating a new protein structure. An average MD structure was calculated over the time range 41–147 ps.

The average MD structure does not show dramatic changes with respect to the starting structure. Indeed, the root mean square (r.m.s.) deviation (defined as described previously[15,29]) with respect to the starting structures is 1.4 Å for all the atoms of the protein, 1.2 Å for the non-hydrogen atoms, and 0.9 Å for the atoms of the backbone. The r.m.s. values reach the equilibrium values before 40 ps and remain stable along the trajectory. They are small with respect to the values reported for other proteins.[15] After equilibration of the protein, the fluctuations of the backbone and of most of the residues are small, indicating an overall rigidity of this system. This has already been observed also for HiPIP from *C. vinosum*,[29] and it is completely consistent with the biological function of these proteins, i.e. electron transfer to another protein. This favorable property of this class of proteins makes us confident in the usefulness of the derived structural model.

The r.m.s. values are, however, somewhat larger than the corresponding values found for *C. vinosum* HiPIP. This is obviously to be expected because of the rearrangements occurring at the backbone and at the side chains of the several residues that have been changed with respect to HiPIP I. A comparison between the backbones of the X-ray structure of HiPIP I and of the MD average structure of HiPIP II is reported in Figure 5.

It should be noted that the largest movements are experienced by the initial part of the amino acid chain, which is lacking in *E. halophila* HiPIP I and has thus been added with a random conformation and initially oriented roughly in the same way as in *C. vinosum* HiPIP. This eight-residue fragment assumes a new position during MD, as the result of the interaction with the rest of the protein. For this particular part of the protein, the r.m.s. deviation tends to increase even beyond the first 40 ps, and it is possible that, even after 147 ps, the equilibrium conformation

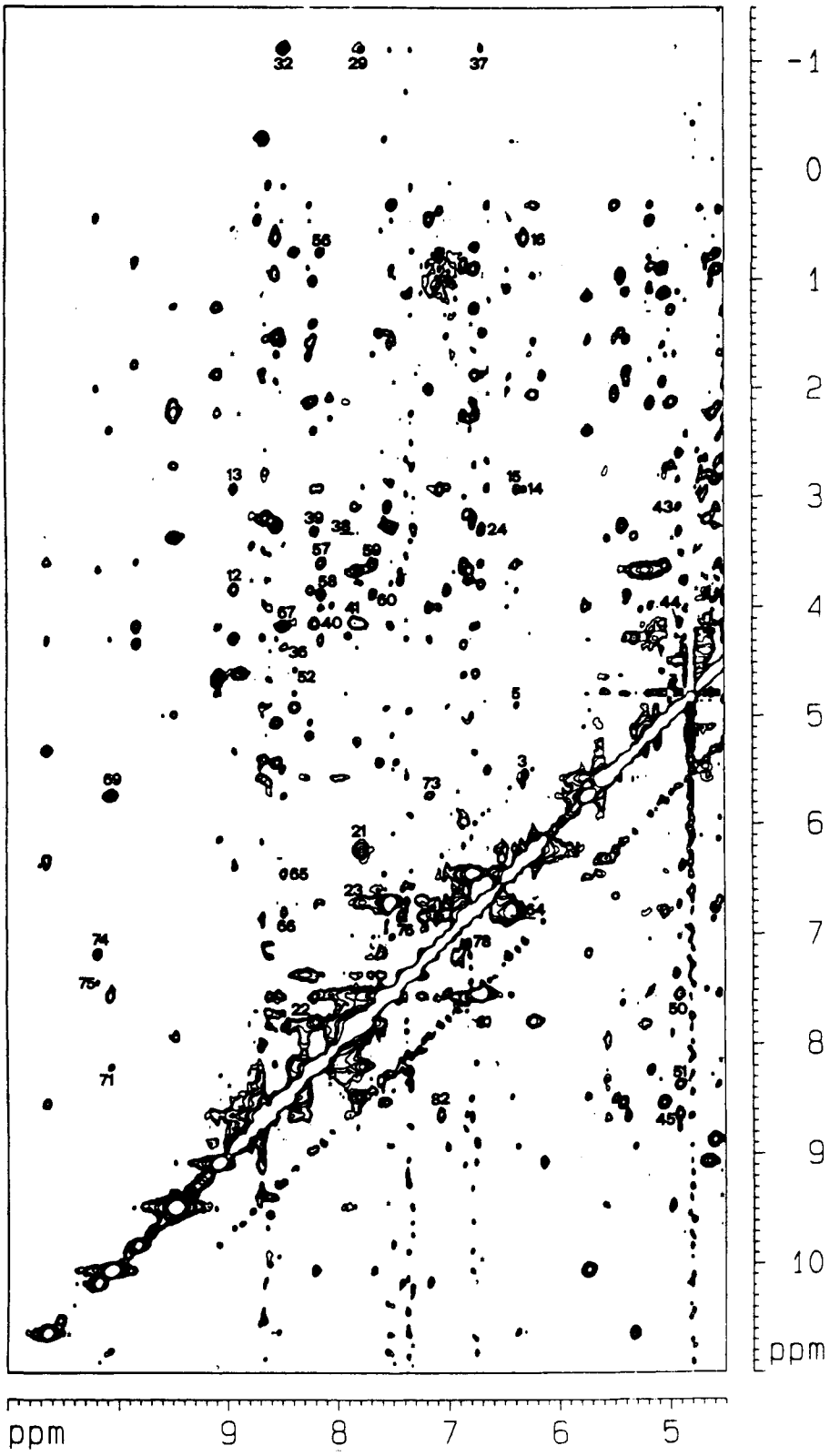

Figure 4. ^{1}H NMR NOESY spectrum (600 MHz, 300 K) of oxidized HiPIP II from *E. halophila*. Conditions as reported in the experimental part. Labeling of the observed cross peaks is reported according to Table III.

has not been attained. Another fragment showing a movement of the backbone involves residues 26–33. This part of the protein undergoes a sideways translation of about 0.5 Å. In both fragments, the movements involve parts of the protein far from the active site cluster. Other minor movements are also detected. In all cases, with only the possible exception of the initial eight residues, the time evolution of the r.m.s. deviation indicates that a stable equilibrium situation is achieved well before the end of the MD run.

It is interesting to note that, even though HiPIP II from *E. halophila* has only 65% homology with HiPIP I from the same bacterium,[14] the tertiary structure can be fully maintained. Furthermore, the aromatic residues around the cluster, which are all conserved, also maintain a very similar arrangement in

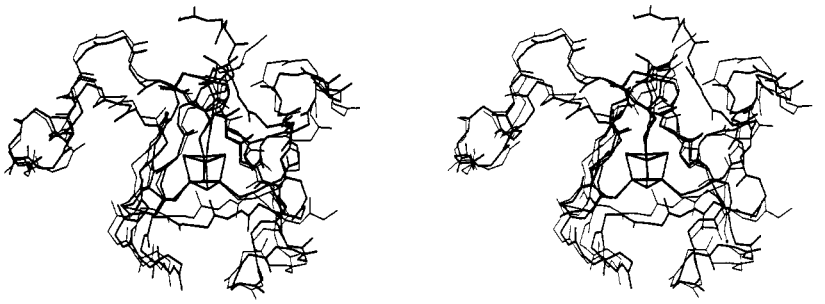

Figure 5. Stereoview of the X-ray structure of *E. halophila* HiPIP I (thin line) compared with the structure of *E. halophila* HiPIP II obtained from MD simulation (thick line).

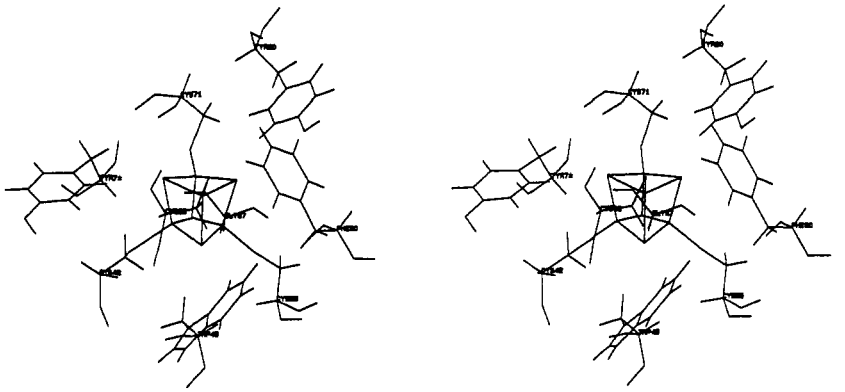

Figure 6. Stereoview of the cluster of *E. halophila* HiPIP II together with metal coordinated cysteines and some aromatic residues around the cluster, whose NMR signals have been assigned.

both systems, i.e. the X-ray structure of HiPIP I and MD structure of HiPIP II. This indicates that the whole protein matrix generates a very similar potential on the residues close to the iron cluster in such a way as to produce similar arrangements of these residues.

Some residues relatively close to the Fe_4S_4 cluster do undergo some rearrangement with respect to the starting structure, in particular Tyr 20, Phe 20, and Glu 40. The location of the side chains of these and other residues around the cluster, whose signals are assigned through NMR, is reported in Figure 6. We have used the present MD calculations to obtain the desired proton–proton distances for our NMR work (Table III). In light of the NMR data, we can state that we have an experimental corroboration of the MD structure of large regions of the proteins, and especially around the active site cluster.

The consistency of the NMR and MD models is for us quite fascinating. It is the first time that the MD approach has been coupled with an NMR investigation involving paramagnetic metal ions, on a protein for which the X-ray structure is not available.

The Charges and Their Distribution in the Cluster of Oxidized HiPIPs. The presence of a ferric pair and a mixed valence pair in the cluster is increasingly becoming a general feature of all oxidized HiPIPs. Although demonstrated by Mössbauer spectroscopy only in the case of *C. vinosum*[2] and *E. halophila* HiPIP II,[11] the same electronic distribution can now be easily deduced from the pattern of hyperfine shifts of HiPIPs from *R. gelatinosus*,[3b,9] *Rhodopseudomonas globiformis*,[33] *Chromatium gracile*,[34] *Rhodospirillum tenue*,[35] and *E. vacuolata* HiPIPs I and II[36] and *E. halophila* HiPIP I.[36] This electronic distribution may or may not be relevant for the function of the proteins. In any case, it was important to ascertain whether the extra electron was shared by the same two iron ions (in a sequence-specific sense) in all these proteins. If so, it could have been inferred that, despite the differences in primary sequence, all the proteins were able to modulate the individual reduction potentials of the iron ions in the same way. The present research has shown that this is not the case. Only the iron ion bound to Cys 43 (*C. vinosum* numbering) maintains a ferric character, and that bound to Cys 63 a mixed valence character on passing from *C. vinosum* (and *R. gelatinosus*) to *E. halophila* HiPIP II. On the contrary, the iron ion bound to Cys 46 becomes part of the mixed valence pair and that bound to Cys 77 becomes ferric. This finding allows us to speculate that the individual reduction potentials are modulated by the proteins in a very subtle way, such that, on passing from one to another, the order may be partly reversed. This pattern may also suggest that equilibrium may exist between a structure in which the second Fe(III) is that bound to Cys 46 and another in which the second Fe(III) is that bound to Cys 77. If such equilibrium were fast on the NMR time scale, we would observe an average situation, the extreme case depicted in Figure 1 being only the more abundant. The equilibrium of two spins would be consistent with the observation of two EPR signals for the oxidized HiPIP from *C. vinosum*.[37] This hypothesis, however, needs further investigation.

The present result seems to indicate that evolution has taken care of the overall reduction potential of the cluster rather than the oxidation numbers inside the cluster itself. Indeed, it may not be important on which side the electron is mainly removed upon oxidation as long as the cluster has the proper potential. It seems however a common feature of all proteins to be characterized in the oxidized state by two iron(III) and a mixed valence pair, the overall redox potential being presumably determined by hydrogen bonds and by the electrostatic potential of each protein atom. The charge distribution within the cluster may also depend on minor variations in bond distances and angles. In this respect it may be worth noting that the Fe–SCys bond distances in *E. halophila* HiPIP I are the following (*C. vinosum* numbering): Fe–SCys 43 = 2.18 Å; Fe–SCys 46 = 2.41 Å; Fe–SCys 63 = 2.09

(33) Bertini, I.; Capozzi, F.; Luchinat, C.; Piccioli, M. *Eur. J. Biochem.* **1993**, *212*, 69–78.
(34) Sola, M.; Cowan, J. A.; Gray, H. B. *Biochemistry* **1989**, *28*, 5261.
(35) Krishnamoorthy, R.; Cusanovich, M. A.; Meyer, T. E.; Przysiecki, C. T. *Eur. J. Biochem.* **1989**, *181*, 81.
(36) Krishnamoorthy, R.; Markley, J. L.; Cusanovich, M. A.; Przysiecki, C. T. *Biochemistry* **1986**, *25*, 60.
(37) (a) Dunham, W. R.; Hagen, W. R.; Fee, J. A.; Sands, R. H.; Dunbar, J. B.; Humblet, C. *Biochim. Biophys. Acta* **1991**, *1079*, 253. (b) Antanaitis, B. C.; Moss, T. H. *Biochim. Biophys. Acta* **1975**, *405*, 262.

Å, Fe–SCys 77 = 2.02 Å. It is known that in $[Fe_4S_4]$ clusters the Fe–SR distances always increase upon reduction,[38] and the observation of the much larger Fe–SCys 46 distance, if conserved in *E. halophila* HiPIP II, would be entirely consistent with our NMR findings, which indicate an inversion of Cys 46 and Cys 77 (*C. vinosum* numbering), the former being more reduced in *E. halophila* HiPIP II than in *C. vinosum*. In *C. vinosum* HiPIP, the corresponding distances vary in the smaller 2.18–2.26 Å range, and the previous considerations cannot be applied to this case.

(38) Berg, J. M.; Holm, R. H. In *Iron-Sulfur Proteins*; Spiro, T. G., Ed.; Wiley-Interscience: New York, 1982; Vol. 4, Chapter 1.
(39) Ambler, R. P. Private communication.

In any case, our results also suggest that the actual electron distribution within the cluster, while being a sensitive reporter of subtle protein-induced effects, may not be relevant for the function of the protein, if proteins like *C. vinosum* and *E. halophila* HiPIP II, with overall reduction potentials differing by about 300 mV, have indeed the same biological function. In any case, a further investigation of analogous systems and more detailed structural information about oxidized and reduced clusters are needed in order to reach general conclusions.

Acknowledgment. This work was supported by C.N.R. Progetto Finalizzato Biotecnologie e Biostrumentezione.